Purdue University

AAE 451: Senior Design Project

Fall 2016 - Team 4

Tube Launched UAS

Final Design Report

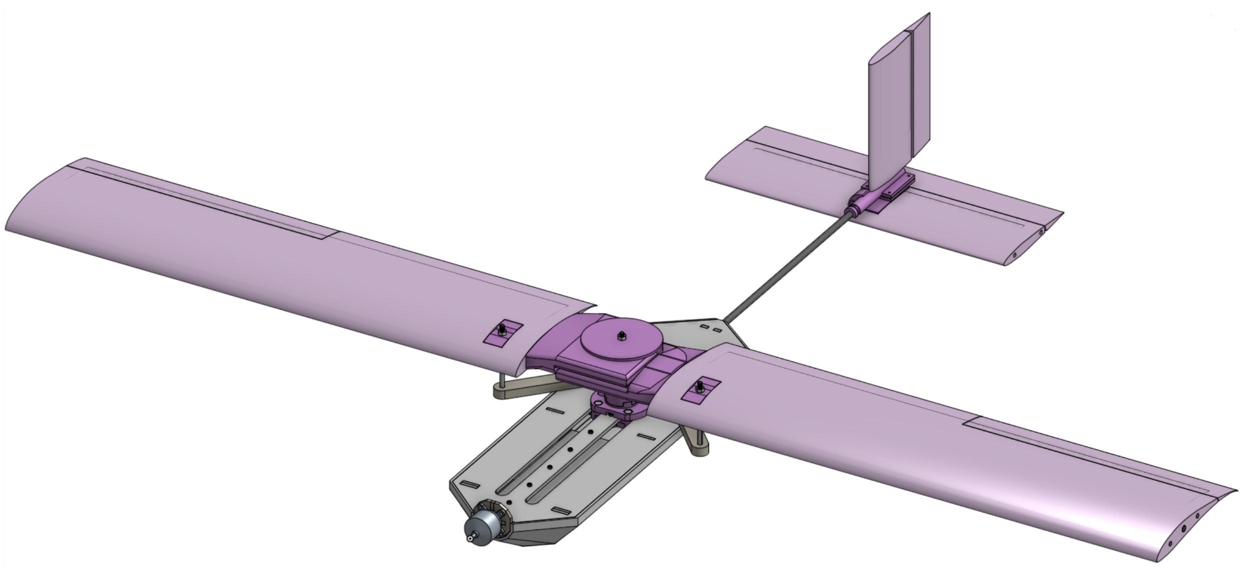

Alexander Flores	______________	Hei (Nancy) Jung	______________
Alex Sechtig	______________	Ujjwal Dalmia	______________
Daniel Ellinwood	______________	Xiao Liu	______________
David Rodriguez-Gutierrez	______________		

Executive Summary

The project involves the design of an Unmanned Aerial System (UAS) that is an electrically powered, remote piloted, tube-launched, fixed wing aircraft. Such UAS are of interest to applications like hazard monitoring, crop observation and cargo delivery. While such tasks are currently being tackled using quadcopters, fixed wing aircraft can provide faster services with a greater range.

The customer put forth a request for proposal (RFP) that outlined the requirements of the project. Some of these design requirements are:

- The launch tube must be no more than 1 ft. in diameter and must not use any chemical explosive means for launch.
- The aircraft must be able to climb to 300 ft. and loiter for at least 8 minutes.
- The aircraft should perform imaging to identify targets placed on the ground.
- The aircraft must land in a skidding mode.
- The aircraft must be capable of being re-launched immediately after landing.
- The aircraft must carry a payload on 0.5 lbs.

Other than these, the RFP also states that the aircraft must be as light as practically possible. It is also required to display Level 1 flying qualities. We were given a budget of $300 alongside the resources available in the Aero Build Lab and at the Aerospace Sciences Lab.

Given these requirements, we designed an aircraft with folding wings and folding vertical stabilizers. The aircraft is estimated to weigh 7.42 lbs and generate a maximum of 0.93 Hp of power. It is designed to cruise at 38.9 ft/s at 300 ft. The maximum load that the aircraft can survive is 3.19 times the weight of the aircraft.

One of the most prominent features of the aircraft is the wing deployment system. This system is designed to move the wings vertically with respect to each other so that they can be level in flight and stacked for launch. The mechanism, which was 3-D printed, is structurally sound and robust.

The system is propelled by a E-Flite Power 32 Brushless motor and a 12x9 folding propeller. Power for launch is provided by surgical tubing connected to fishing line that extends 100 ft. outside the tube; this system was inspired by a high start system commonly used for radio control gliders. Overall, the aircraft is expected to use 60-65% of the energy available to complete the mission which involves climb, loiter for 8 minutes and landing.

Table of Contents

Concept Selection and Initial Sizing

Concept Selection

The very first stages of creating the design was a team-based concept selection session. As a group, we took potential ideas from all of our individual designs and condensed them into three possible designs for consideration. The morphological matrices defining the characteristics of each of these three designs are available in the Appendix, and below is a brief description of each concept:

- **Concept 1:** This concept had a rocket-like fuselage with a pusher-prop located at the rear of the aircraft. In addition, the main wings were triangular in shape and composed of 3 main parts: a folding carbon fiber rod acting as the leading edge, a nylon fabric sheet acting as the main surface of the wing, and a folding foam piece acting as the trailing edge and containing our control surfaces.
- **Concept 2:** This concept was a slight variation on Concept 1 that replaces the carbon fiber rod with another rotating foam section to act as the leading edge. This would require and the 2 foam sections to somehow be stacked on top of one another when un-deployed and changes the overall wing=shape to rectangular. In addition, the pusher-prop has been replaced by 2 EDFs located at the rear of the aircraft.
- **Concept 3:** This concept simplifies the wing deployment system of the other 2 concepts by utilizing 2 solid foam wings stacked on top of each other and rotationally deployed from a single point on the top of the fuselage. This deployment required a screw-like mechanism in order to raise or lower one of the wings with respect to the other in order to have both wings completely level once fully deployed.

We created a Pugh matrix, seen in table 1, in order to evaluate each of the 3 concepts and determine how well they accomplish our intended goals and our given requirements.

Table 1: Pugh Matrix

Evaluation Criteria	Subsystems Affected (0 = No, 1 = Yes)				Weight (1 - 5)	Score (1 - 5)		
	Aerodynamics	Structures	Propulsion	Controls		Concept 1	Concept 2	Concept 3
Wing Deployment Time	0	1	0	1	3	2	3	3
Aspect Ratio	1	1	0	0	4	3	1	5
Internal Volume for Wings and Tail	0	1	0	0	1	4	3	1
Internal Volume for Components and Payload	0	1	0	0	3	4	2	4
Propeller Diameter	1	0	1	0	3	5	4	2
Stall Characteristics	1	0	1	1	4	2	4	5
Launch Stability - Response Settling Time	1	1	1	1	4	4	4	2
Low Cruise Speed	1	0	1	1	3	3	4	5
Aircraft Weight	0	1	1	0	4	4	3	2
Adherence to Budget Ease	1	1	1	1	3	3	2	5
Controllability/Handling	1	0	1	1	4	3	3	3
Reliability of Wing Deployment System	1	1	0	1	5	2	1	4
Wing Manufacturability	1	1	1	1	3	3	3	4
Fuselage Manufacturability	0	1	0	0	2	2	2	3
Folding Mechanism Manufacturability	1	1	0	1	4	3	3	2
				Aerodynamics Total		112	104	136
				Structures Total		110	86	119
				Propulsion Total		94	95	96
				Controls Total		91	97	119
				Grand Total		407	382	470

Based on the weights of various design criteria, Concept 3 was determined the best design to meet the requirements for this project. Thus, we selected Concept 3 as our initial design and began shaping our individual sub-systems based on its characteristics.

Initial Weight Estimate

The initial weight of the aircraft was determined by making a few basic assumptions about the performance characteristics of the aircraft, defining and analyzing the mission profile, and then comparing the battery and payload weight to historical values.

The assumed performance characteristics are:

- Cruise Velocity: 40 ft/sec
- L/D_{max}: 6
- Propulsion Efficiency: 0.44
- Battery Energy Density: 2.39E5 J/lb
- Turn Radius: 50 ft.
- Climb Angle: 20 degrees
- Endurance: 20 min
- Percentage of loiter time spent level: 25%

The flight mission profile is broken up into three distinct parts: climb, level loiter, and turning loiter. Using the assumed performance characteristics above, a necessary battery weight to aircraft weight fraction was calculated and then summed for each part of the mission profile. Then, the initial weight estimation can be found by comparing the fraction of the total battery plus payload weight and aircraft weight to the historical data. The figure below shows that the intersection of the estimated weight line and the historical weight line gives an initial weight estimation of 5.12 lbs.

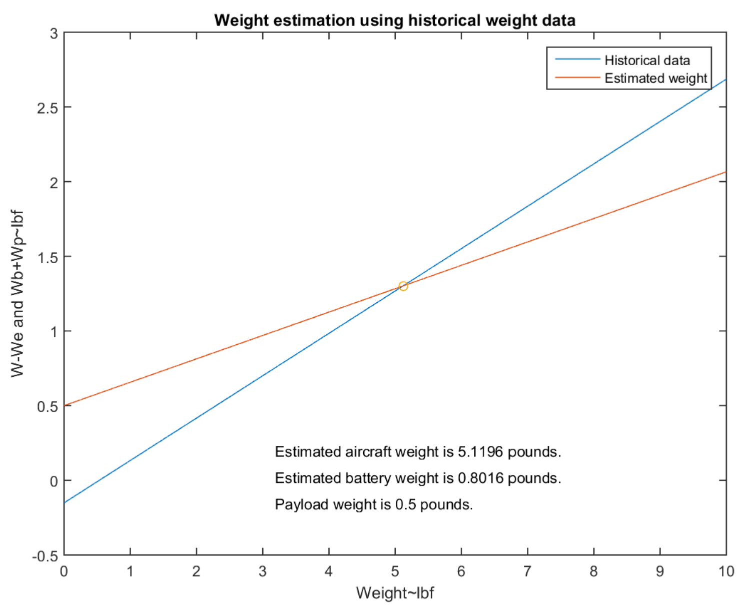

Figure 1: Estimated weight compared to historical weight data

Constraint Diagram

The constraint diagram was determined by making a few more basic assumptions about the performance characteristics of the aircraft and using them to determine constraints based on stall, cruise, and climb characteristics.

The additional assumed performance characteristics are:

- Stall Velocity: 30 ft/sec
- C_{Lmax} Range: 1.4 – 1.6
- C_{D0} Range: 0.03 – 0.07
- L/D_{max} Range: 5 – 9

Figure 2 below shows the stall, cruise, and climb constraints in addition to the initial and final design points. The design space is constrained to a power loading of less than 12.88 lbf/hp and a wing loading of less than 1.49 lbf/ft. The initial design point had a power loading of 7.5 lbf/hp and a wing loading of 1.3 lbf/ft. After a detailed design of the sub-systems, discussed below, the final design has a power loading of 9.6 lbf/hp and a wing loading of 1.45 lbf/ft.

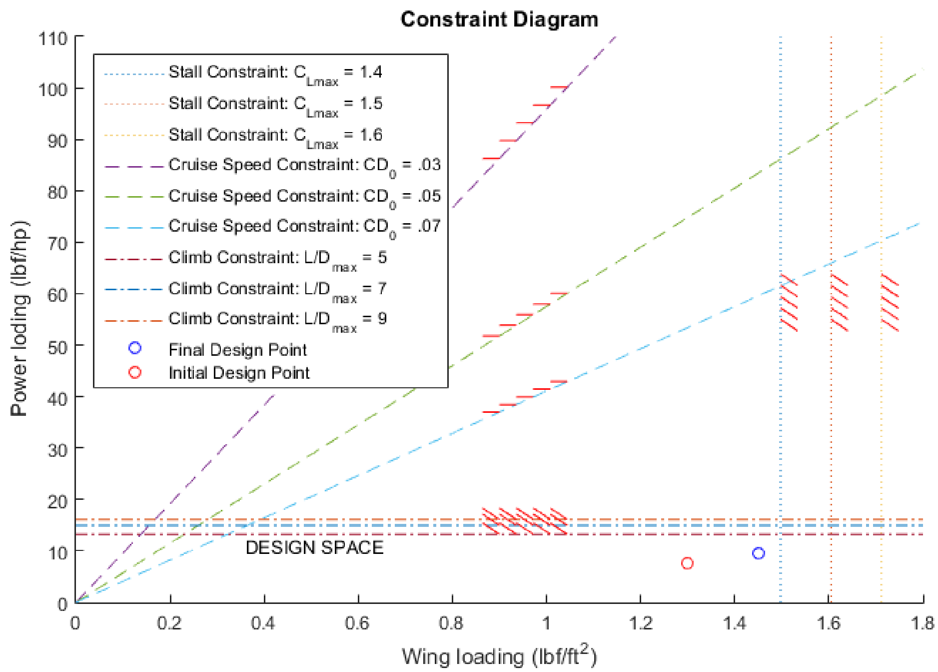

Figure 2: Constraint Diagram

Launch and Wing Deployment

The launch system selected for this mission resembles a High Start Launch System. The system includes an 8 ft. long tube that houses the aircraft in its entirety. The aircraft is connected to a fishing line using a hook and the fishing line is connected to surgical tubing that provides the force to launch the aircraft. An illustration of the system can be found in Figure 3.

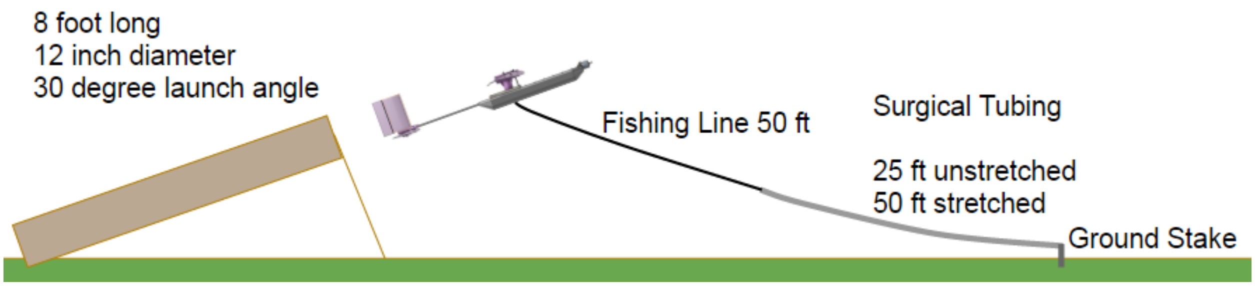

Figure 3: Launch System Overview

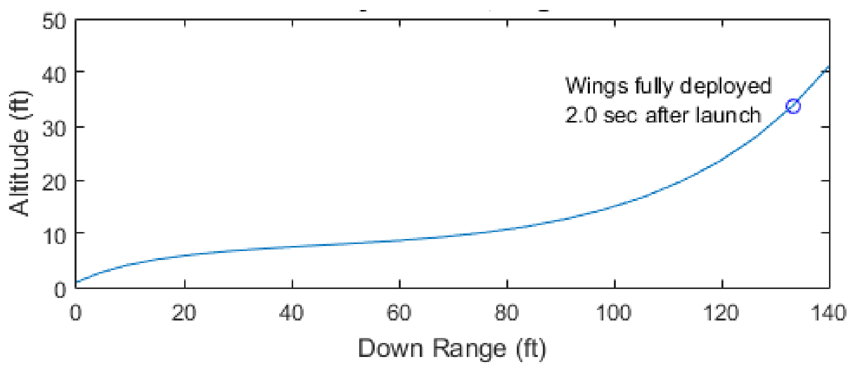

Figure 4: Flight profile at launch

Figure 4 shows the flight profile, where 0 ft. on the x axis is the exit of the tube. The aircraft will be launched at a 30° angle and is predicted to exit the tube at 38.9 ft/s. The high start system provides a forward force to the aircraft until 25 ft. downrange and the aircraft continues to fly with wings moving into the final position. The simulation accounts for the change in aerodynamic characteristics of the aircraft in the transient phase from launch to fully deployed.

The wing deployment system consists of four major unique components: wing mounts, spiral rotator, slider bar and positioning bars. These can be seen in figure 5. The movements of the system can be visualized in Figure 6. The spiral rotator is pulled back by surgical tubing, when it pulls on the wings, the positioning bars make the wings rotate into position.

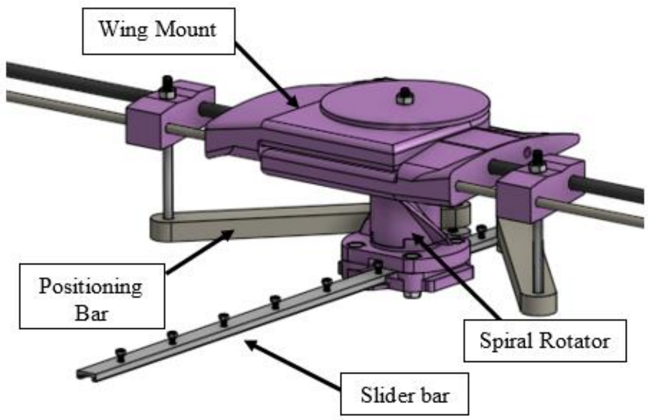

Figure 5: Components of the wing deployment system

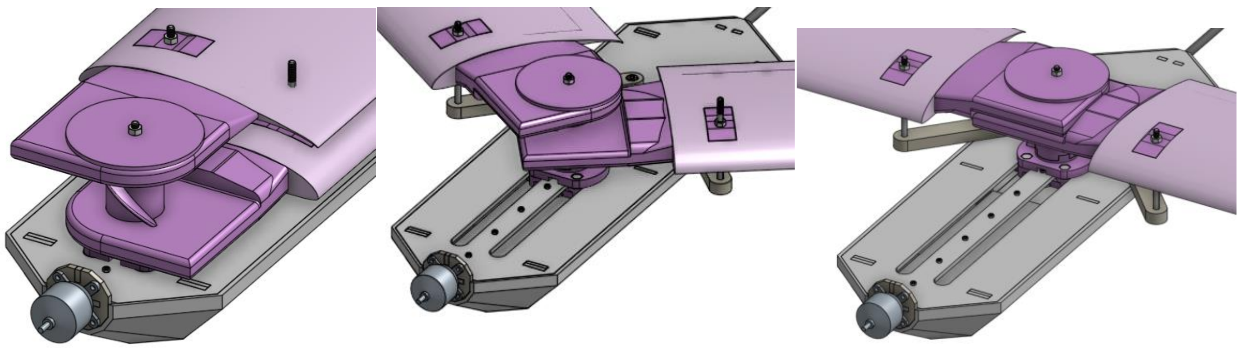

Figure 6: Wing deployment system movement

This complex launch mechanism was warranted for the mission due to multiple reasons. Since the tube diameter is fixed and the wings need to fit inside the tube, the wings had to move vertically with respect to each other so that the chord could be larger. It was important to have a larger chord so we could have structurally sound wings and at the same time meet the wing loading constraint.

Finally, a folding mechanism is required for the horizontal stabilizer since the span is larger than the diameter of the tube. This is a simple mechanism with one rotation point as seen in figure 7. The rotation is powered by surgical tubing and the horizontal stabilizer is held in position by magnets.

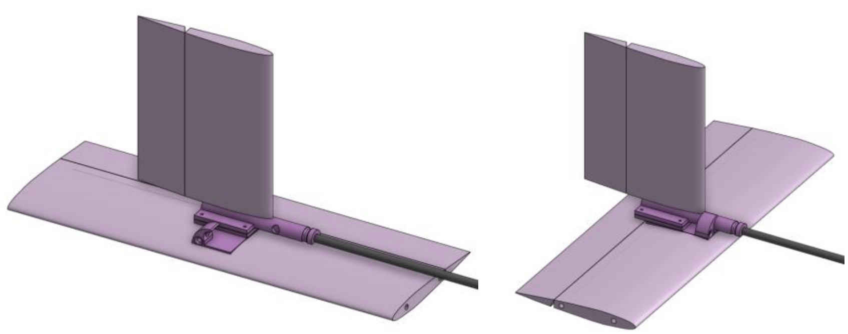

(a) Inside tube (b) Deployed

Figure 7: Horizontal stabilizer deployment system

Propulsion

Introduction

Before any major analysis was performed, the guidelines from the RC community were considered to estimate the approximate size of a motor from our preliminary weight estimation. With an initial weight estimation of about five to six pounds, the RC community recommends that for a trainer/slow flying scale models, it is best to use between 70 to 90 watts per pound to properly fly the aircraft. The motor's power estimation is then ranged between 350 to 540 watts (0.46 Hp to 0.73 Hp).

Propeller - Motor Selection

The process to select the propeller began by computing the thrust required to fly the aircraft at a cruise velocity of 38 ft./s, as determined by the aerodynamics team. Using the thrust required to cruise in steady-level flight, the power absorbed and the efficiency of each propeller at cruise conditions were noted; experimental propeller data from UIUC (University of Illinois Urbana-Champaign) and APC (Advanced Precision Composites) were used to analyze the propellers within the databases. Initially, a 9x7 propeller was decided to be sufficient but due to the large RPM required and the small motor that compliments it, the system was not recommended for the updated weight of about seven pounds. Using the propeller data, the Figure 8 was generated by plotting the power absorbed for each propeller versus the corresponding efficiency of that propeller at our given cruise flight conditions. The propeller selected is the 12x9 folding propeller due to the low power required and high efficiency.

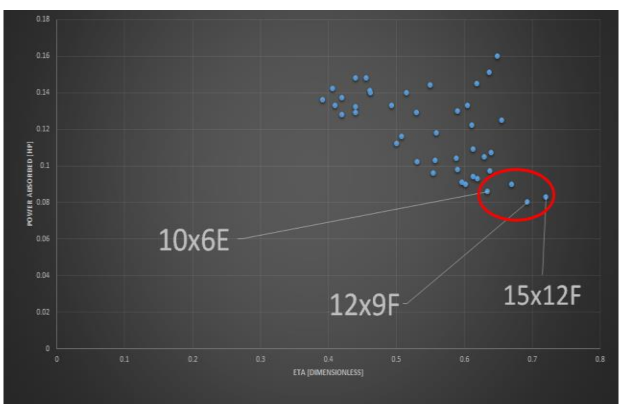

Figure 8: Efficiency vs Power Absorbed

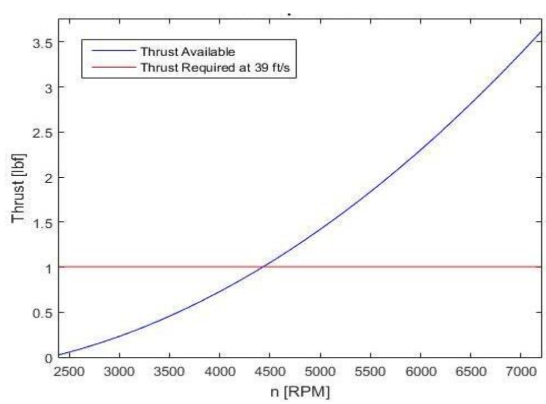

Figure 9: Thrust Required vs RPM

Now, the correct motor needed to be sized in order to properly run the propeller. The geometric properties of the 12x9 folding propeller were noted by measuring the propeller itself. The data was then input into the gold.m code to theoretically determine the coefficient of thrust and power as a function of RPM while the velocity remained constant at the cruise velocity. This procedure was performed to estimate the required RPM of the motor to cruise as shown in figure 9.

In order to validate the RPM of the motor during cruise, another set of data was extrapolated from the gold.m code that was provided to us at 4400 RPM and now the velocity was varied to determine the coefficient of thrust, power and the advance ratio. The Main_System_Design.m code, which was also provided, was then used to determine a realistic rotation rate. An RPM of

4587 requires that the propeller absorbs 77 watts of power which is required to be outputted by the motor.

Climb analysis is analogous to cruise; however, the equations of motion are different due to the flight path angle not being equal to zero during climb. Since the RPM of the motor during cruise was estimated to be about 4587, an RPM of 6000, 7000, and 8000 were used to determine the best climb conditions. To analyze the propulsion system during climb, the power available and power required were plotted over a range of velocity to determine the excess power available as shown in figure 10. The excess power can be used to determine the climb rate which confirms that our UAV will climb to 300 feet in the space provided by McAllister Park.

The efficiency of the propeller is also used to determine the best RPM during climb. At 6000 RPM the climb rate was not sufficient but the efficiency was highest. At 8000 RPM the efficiency was the lowest and the climb rate was not much greater than at 7000 RPM. At 7000 RPM, the efficiency and climb rate were sufficient for the mission and thus 7000 RPM was selected. At 7000 RPM the propeller absorbs 323 watts which is the determining factor when deciding which motor to use.

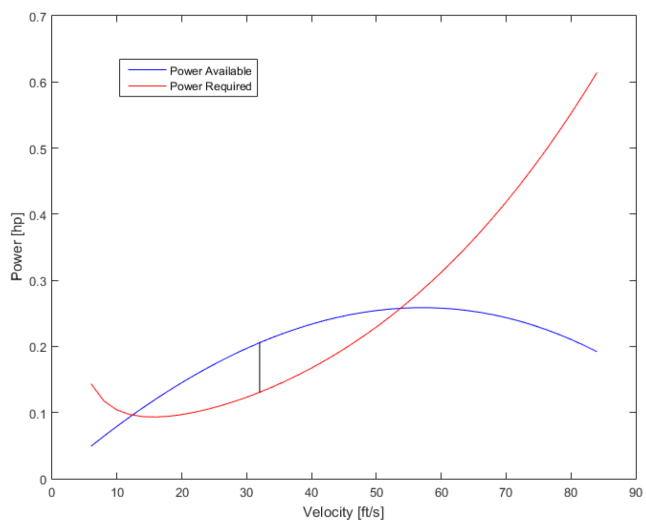

Figure 10: Power Available/Required vs Velocity during Climb

The E-Flite Power 32 Brushless motor can produce 693 watts of power which is larger than the power absorbed by the motor during cruise and climb conditions. The second reason the Power 32 motor was selected is because the folding propeller is recommended to be used with a motor which can produce at least 450 watts of power. Both are satisfied with the Power 32 Brushless motor.

A test of the propulsion system was performed with a test stand provided in the build lab. The static thrust test performed verified that the system was properly connected and thrust was noted to assure that the correct amount of thrust can be produced during flight.

Electric Speed Controller Selection

An electric speed controller is categorized by two main parameters, the max voltage and the max current draw. The motor has a max current draw of 60A, thus the speed controller needs a max current draw of 60A as well to avoid under powering the motor during flight. The motor also requires a voltage between 12 and 16 which means the ESC must have a max current of 16 volts as well.

Battery Analysis

The requirements for a battery are that the battery must produce at least 12 to 16 volts as required by the Power 32 Brushless motor and the total current that can be drawn from the battery must be greater than the max current draw of the motor and ESC. The battery must contain enough energy to climb to 300 feet, sustain eight minutes of steady-level flight, and power the servos and camera/telemetry components. Using the range of volts required by the motor and knowing that each Li-Po cell provides 3.7 volts, the motor needs at least 4 cells which is a total of 14.8 volts.

The battery capacity size was determined by evaluating the time that the battery can used for. Battery endurance was evaluated by dividing a range of battery capacities in ampere-hour by a range of available current inputs. Using the Main_System_Design.m code, I was able to determine the current drawn by the motor at our given cruise conditions. The current drawn from the battery was calculated to be 7.7A, which means that an 1800mAh battery will provide 8 minutes of steady-level cruise flight. Using a factor of safety of 100 percent, the capacity of the battery was selected to be 3600mAh; the factor of safety included the cold weather effect on the battery and the unknown power consumed from the servos and camera. Because we are using a high-start launch system, the energy consumed during climb is reduced.

Finally, the discharge rate was determined by dividing the max current by the capacity of the battery. The maximum discharge rate was calculated to be 16.3, which means that a 15C discharge rate is required to avoid under powering the motor via the ESC. Overall, the battery required is a 4S 3600mAh 20C LiPo battery. However, due to the long shipping time of a battery with the current specifications a battery of 3000mAh will be used instead.

Summary

The components that were decided on were the Aeronaut 12x9 CAM Carbon Fiber Folding propeller with a E-Flite Power 32 Brushless Outrunner. The battery in concert with the propeller-motor subsystem is a Turnigy 3000mAh 4S 20C Li-Po battery along with a Hyperion 15V 60A ESC.

Table 2: Propeller, ESC Properties, Motor, and Battery Properties

Propeller Properties		**Electric Speed Controller Properties**	
Diameter	12 in.	Max Voltage	15 V
Pitch Thickness	9 in.	Max Current	60 A
Airfoil Shape	An optimized thin blade section with a wide chord		
Motor Properties		**Battery Properties**	
Max Horsepower	0.93 Hp	Input Voltage	14.8 V
Motor Efficiency	0.828	Capacity	3000 mAh
Weight	0.335 lbs.	Discharge Rate	20 C
Kv	770 RPM/Volt	Number of Cells	4S
Idle Current (Io)	2.00A @ 10 V	Battery Type	Lithium Polymer

Aerodynamics

The primary design objective for the aerodynamics system is to generate enough lift to keep the aircraft flying. It is also important that the aircraft is stable and maneuverable in flight in order to display the level 1 flying qualities required in the RFP. The aerodynamic characteristics also affect efficiency and power required for flight. An additional consideration for this project was to ensure the stall speed is low so that the launch system can provide the vehicle with enough velocity to take off.

Main Wing

A major constraint on the main wing design was the size of the wings since the entire aircraft needs to fit in a tube. Based on this, the size constraints on the wing were: a maximum chord of 9.5 in and a maximum thickness of 1.25 in. Based on manufacturing constraints, the minimum thickness required was 0.25 in in order to fit a spar. Finally, wing area was constrained as shown in the constraint diagram.

Airfoil Selection

Using some initial estimates of velocity and chord length, the Reynolds number was estimated to be 200,000. Based on this, we surveyed Selig's Summary of Low-Speed Airfoil Data Volumes 1-3 for airfoil performance characteristics at Re = 200,000. With this data, the process in Figure 11 was followed.

The final airfoil selected was the S1210, which can be seen in Figure 12. Figure 13 shows the c_l vs α plot published in Summary of Low-Speed Airfoil Data, Volume 1.

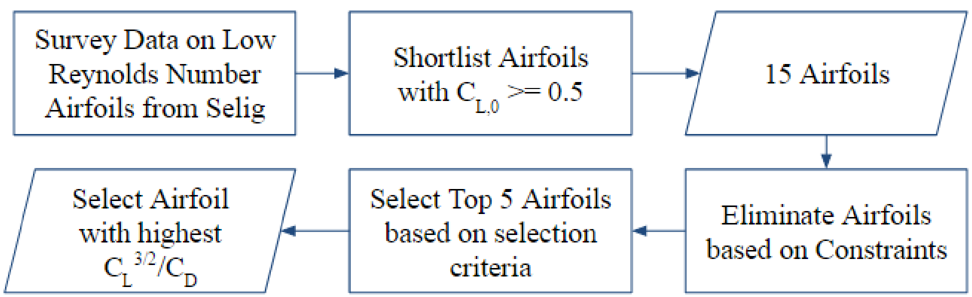

Figure 11: Airfoil selection process

Table 3: Airfoils considered for main wing.

Airfoil	$c_{l,0}$	c_d **at α = 0**	$c_{l,max}$	$c_l^{3/2}/c_d$ **at α = 0**	c_l/c_d **at α = 0**
NACA 6409	0.6	0.012	1.35	38.73	50.00
FX 63-137	0.7	0.016	1.6	36.60	43.75
S1210	**0.9**	**0.016**	**1.9**	**53.36**	**56.25**
E423	0.95	0.022	2	42.09	43.18
SG6043	0.7	0.016	1.5	36.60	43.75

Figure 12: Cross Section of the S1210

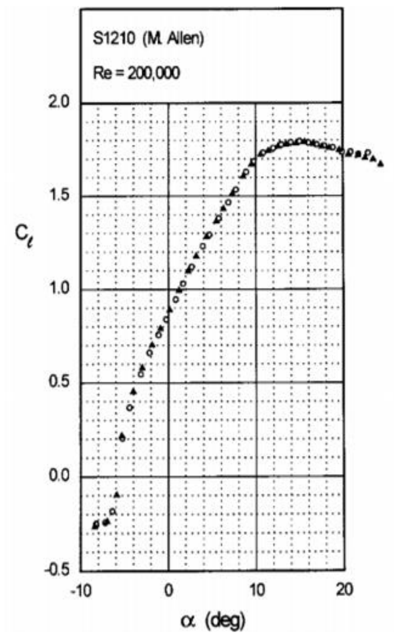

Figure 13: S1210 c_l vs α

The challenge with the S1210 was manufacturing the slender trailing edge. This was tackled by using a modified airfoil with a thicker trailing edge as input to the hot wire cutter to get the desired airfoil as the output.

3-D Wing Design

The wing planform area was based on the estimated weight of the aircraft and the wing loading constraint. Table 4 contains the 3-D design characteristics for the aircraft.

Tapered wings were considered to improve the efficiency of the wings; the idea was not implemented since tapered wings would have to be longer, and due to the folding nature of the wings, that would require a longer fuselage, adding weight. The added complexity in manufacturing was another reason to not add tapered wings.

Table 4: 3-D wing design

Chord Length	9.5 in
Span	77.118 in
Taper Ratio	1.0
Sweep Angle	0.0
Aspect Ratio	8.10
Dihedral Angle	0.0

In order to improve roll stability, we considered adding a dihedral to the wings, making the system inherently stable. While wings with dihedral could be accommodated in the wing deployment system, the final design does not have any dihedral; this decision was based on the fact that it would be difficult to manufacture such a structure.

Tail Design

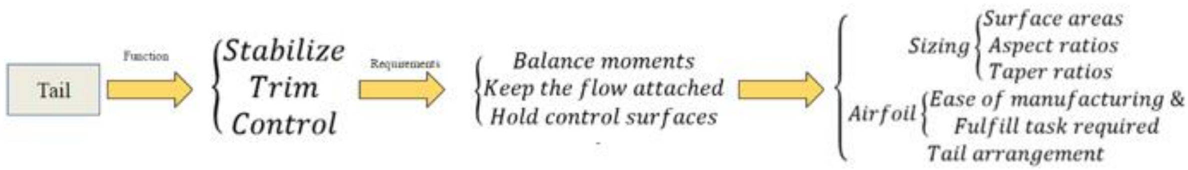

Figure AERO14: Tail design and sizing process

The basic functions of a tail have been summarized in figure 14. Due to the unique design challenge posed by the tube launch requirement, we considered two different tail arrangements. The advantages and disadvantages of these can be seen in figure 15. The conventional arrangement is the lightest possible configuration, as all the stabilizers are directly attached to the fuselage. The major advantage of the twin tail is that by having two vertical stabilizers, each of the vertical stabilizers can be half the height.

$$Tail\ Arrangement \begin{cases} Conventional\ tail \begin{cases} Adv. \begin{cases} Ligthest \\ Structurally\ convenient \end{cases} \\ Disadv. \{ Folding\ difficulties \end{cases} \\ Twin\ tail \begin{cases} Adv. \begin{cases} Height\ reduction \\ Ease\ of\ folding \end{cases} \\ Disadv. \{ Heavier \end{cases} \end{cases}$$

Figure 15: Tail arrangement trade study

The CAD model demonstrated that a conventional tail configuration could be successfully fit in the tube. The conventional tail was selected due to its simplicity and lower weight.

Finally, the NACA 0012 was selected as the airfoil for both the horizontal and vertical stabilizer. The 12% thick airfoil provides enough room for control surfaces while the symmetric shape provides a simple and effective design.

Parasite Drag Estimate

The method used to estimate parasite drag is described in Raymer, p. 280-289. The formula used is shown in equation 1. In this equation C_f is the skin friction coefficient, which varies for turbulent and laminar flow, FF is the form factor, Q is the interference factor, assumed to be 1 for all components, S_{wet} is the component's wetted area, and S_{ref} is the aircraft's wetted area. It was assumed that the flow over the wings and tail is laminar, and the flow over the fuselage is entirely turbulent since it is in the wake of the propeller.

$$C_{D,0} = \frac{\sum(C_{f,c}\, FF_c Q_c S_{wet})}{S_{ref}}$$

Equation 1: Parasite drag estimate.

The relations for the variables can be found in Raymer. The parasite drag based on this analysis was $C_{D,0}$ = 0.027.

Computational Fluid Dynamics Analysis

Preliminary aerodynamic analysis was performed using XFLR5. Details of this can be found in the appendix. Since the wing span of the airplane (77") is larger than the width of the Boeing wind tunnel (72") available to us, we could not perform wind tunnel tests. Thus, in order to get more reliable data on the aerodynamics of the aircraft, CFD analysis was performed using Star-CCM+. The results of the analysis can be seen in Table 5. Figure 16 shows pressure distribution over the aircraft at $\alpha = 0°$ along with streamlines. Details of this analysis can be found in the appendix. Table 5 provides a summary of the aerodynamic characteristics of the aircraft.

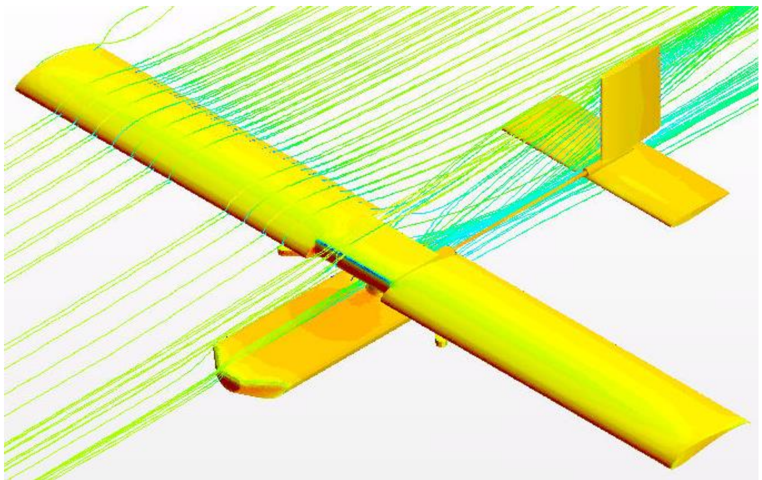

Figure 16: Pressure and streamlines over the aircraft

Table 5: Aerodynamic characteristics of the aircraft

Variable	**Value**
$C_{L,0}$	0.46
$C_{L\alpha}$	0.082
$C_{L\delta e}$	0.0086
$C_{D,0}$	0.080
k	0.047
C_{M0}	-0.018
$C_{M\alpha}$	-0.012
$C_{M\delta e}$	-0.0060
Aerodynamic center	4.56 (x/c)
$C_{L,max}$	1.5
α_{stall}	15°

Structures

This section of the report will focus on outlining the overall process and analyses performed in order to design our aircraft's structural components and their material composition. Overall, the design process focused on making the aircraft as light as practically possible while still maintaining the strength required to endure the maximum loading conditions that will be endured by the aircraft during its mission. While much of the design was initially analyzed during the flight portion of the mission, the mission requirements of being tube-launched and performing a belly landing required additional analysis in order to ensure structural integrity of the aircraft during these two critical phases.

Weight Estimate

We have a total estimated aircraft weight of 7.42lbs. The weight of the aircraft was determined by the components listed in Table 6 below. Figure 17 shows a pie chart of the distribution of the weight of the aircraft.

Table 6: Weight Estimation of each component

Main Component	Weight(lbs)	Material
Main Wings and Tail	2.332	• Pink Foam • Fiberglass • Carbon Fiber Tube • Hardwood Dowels • 3D Printed Plastic
Fuselage	0.875	• Foam board • Hardwood Board
Folding Mechanisms	2.044	• 3D Printed Plastic
Propulsion System	1.57	• Motor • Battery • Propeller • ESC
Camera	0.15	
Payload	0.5	
Total Weight	**7.42**	

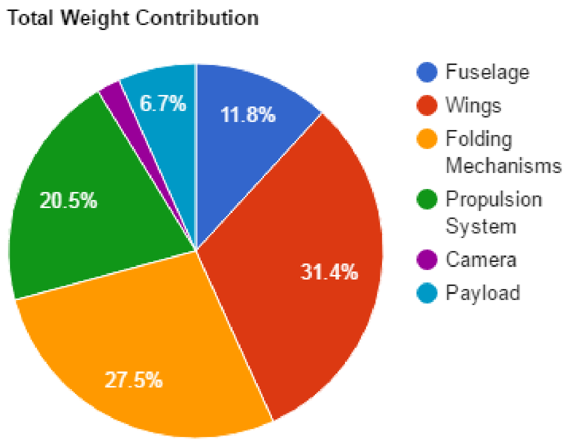

Figure 17: Total Weight Contribution

Load Path Diagram

In order to facilitate what kinds of analyses we would need to perform to determine if our aircraft would be able to endure its mission, we first created a load path diagram to visualize the major loads our aircraft would endure and where they would be located, as shown in Figure 18.

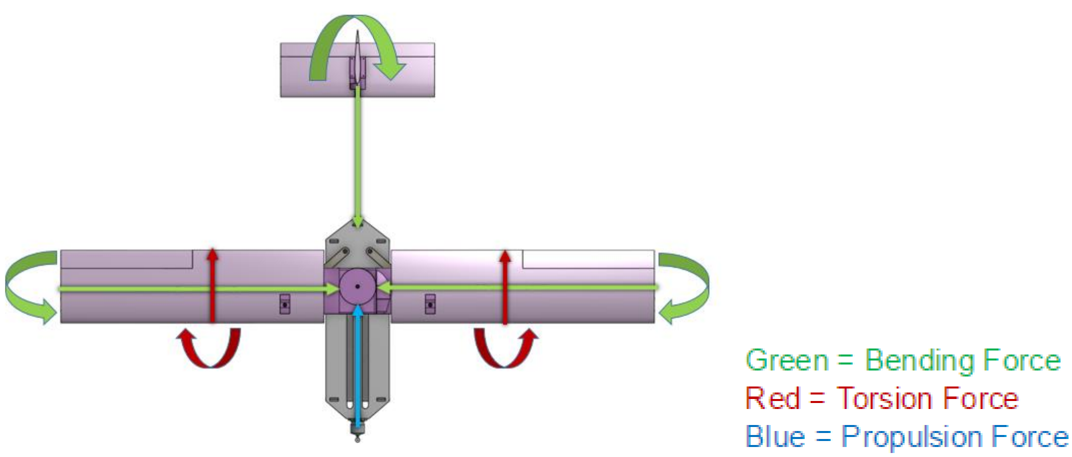

Figure 18: Load Path Diagram

In order to determine the magnitude of these forces, we had to determine our maximum load factor.

Maximum Loading Conditions

For the flight portion of our mission, the maximum loading conditions would occur when the aircraft is traveling at its maximum velocity and performs a sharply banked turn. Based on our maximum velocity of 46 feet per second, an intended turn radius of 35 feet, and a safety factor of 1.5 (standard in structural analysis), the bank angle, maximum load factor, and maximum bending moment of our main wings were found as shown in Table 7.

Table 7: Maximum Loading Conditions

Parameter	Value	Units
Maximum Load Factor	3.19	N/A
Maximum Lift Force	23.6	lbf
Maximum Bending Moment	201	lbf-in

Now that we had determined our maximum loading conditions and where they would occur, we could proceed by performing individual sets of analysis on key points in the design in order to determine that they would not break.

Main Wing Analysis

For our main wings, our analysis was split into three sub-sections: spar sizing, skin thickness from bending, and skin thickness from torsion.

Spar Sizing

In order to determine the minimum size of carbon fiber tubes we would need to use for our main wing spars so they would not break under maximum loading, we chose to analyze our spars as simple, cantilever beams under the assumptions of uniform loading at maximum conditions, as shown in Figure 19.

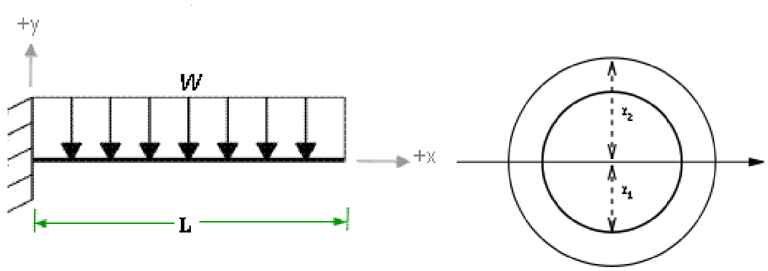

Figure 19: Cantilever Beam Assumption and Cross-Section

By doing so, we were able to determine the maximum bending moment the wings would endure and the minimum dimensions required for a hollow carbon fiber tube to withstand this moment. In addition, the maximum deflection of the wing was calculated to further ensure that, besides not breaking, the wings would stay fairly un-deformed during maximum loading. The results of this sizing for our selected carbon fiber tubing is shown in Table 8.

Table 8: Spar Analysis Results

Parameter	Value	Units
Maximum Stress Endured	67.3	Ksi
Ultimate Material Strength	160	Ksi
Maximum Tip Deflection	4.49	Inches
Maximum Tip Deflection Angle	7.56	Degrees

As shown in Table 8, our carbon fiber spars will be able to endure our maximum loading conditions with only minimal deflection and without breaking. In addition, these deflections will likely be even lower during our actual flight due to the overestimation of our bending moment due to our safety factor and evenly distributed loading assumption.

Skin Thickness from Bending and Torsion

In order to determine the minimum amount of fiberglass our wings would require in order to endure the large bending moments and torsional forces created during flight, we chose to assume our wings were rectangular in shape and that the thin skin around the wing would take all of the loading, as shown in Figure 20.

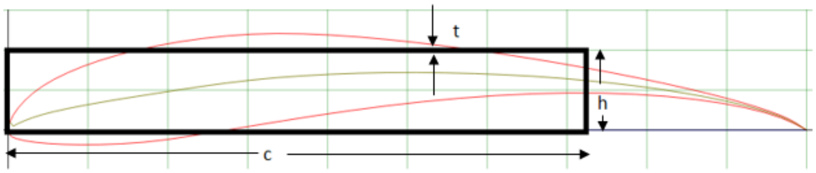

Figure 20: Rectangular Cross-Section Assumption

By doing so, we were able to use the maximum bending moment and maximum torsional force equations to determine the minimum skin thickness required of our fiberglass. Both of these values were used to determine the number of layers of fiberglass our main wings would require. The results of this sizing analysis is shown in Table 9.

Table 9: Skin Thickness Analysis Results

Parameter	Value	Units
Minimum Skin Thickness (Bending)	0.00021	inches
Minimum Skin Thickness (Torsion)	0.00898	inches
Single Layer Thickness	0.01563	inches

As these results clearly show, largely due to our inclusion of main wing spars, our aircraft's main wings only require a single layer of fiberglass and resin in order to not break under maximum loading conditions.

Tail Boom Analysis

For our carbon fiber tail boom, our analysis was split into two sub-sections: in-flight and a worst-case landing analysis.

In-Flight

In order to ensure our carbon fiber tail boom was sized correctly in order to not break under maximum loading conditions, we chose to analyze our tail boom as a simple cantilever beam with a point-load applied anchored at two points within our fuselage, as shown in Figure 21.

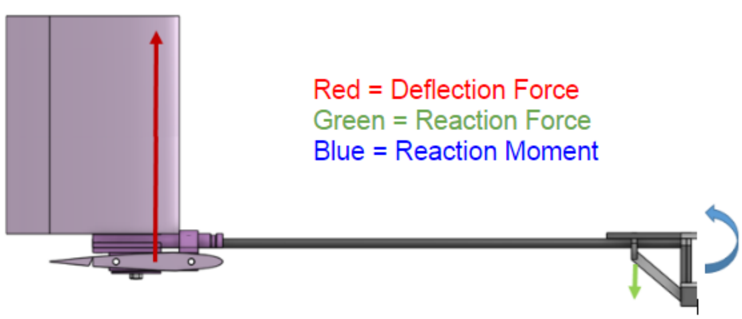

Figure 21: Tail Boom Point-Loading Assumption

By using an XFLR5 approximation and a large safety factor, we determined a maximum deflection force that would be caused by our horizontal stabilizer during flight. Using this loading, we were able to determine the maximum bending moment in the tail boom and, therefore, the maximum stress and deflection of the boom, as shown in Table 10.

Table 10: In-Flight Tail Boom Analysis Results

Parameter	Value	Units
Maximum Stress Endured	60.3	ksi
Ultimate Material Strength	160	ksi
Maximum Boom Deflection	1.51	inches
Maximum Boom Deflection Angle	4.21	degrees

From these results, it is clear to see that our carbon fiber tubing is adequately sized for our tail boom in order to create minimum deflections and not break under maximum loading conditions.

Landing Analysis

In order to ensure our tail boom could survive a direct impact with the ground, we assumed conservation of total energy of the system to determine the maximum point-force that would be generated from a direct strike into the ground during a controlled landing of our aircraft. Because this calculated force was found to be 8.61 pounds and our in-flight analysis assumed a maximum deflection force of around 10 pounds, the stresses and deflections created by this impact would be less than those shown above in Table 4. Therefore, our tail boom sizing is also more-than-adequate to survive a direct impact with the ground during a controlled landing.

Fuselage Analysis

In order to ensure our fuselage can endure various extreme portions of our mission, we chose to focus on analyzing our fuselage during a belly-landing and during launch.

During a belly landing, it was assumed that the wooden channel running along the bottom of our fuselage would endure the brunt of the impact loading and conservation of energy was used to determine the actual force of that impact located at the worst-case, least supported point along this channel, as shown in Figure 22.

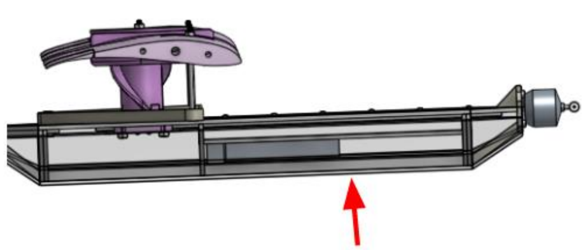

Figure 22: Belly-Landing Impact Assumption

By using these assumptions, a maximum bending moment acting on the hardwood channel was found and a corresponding maximum stress as well.

During launch, our aircraft will be pulled by a stretched piece of tubing from a small hook anchored at the front of our fuselage directly into a hardwood riser. The hook will be located directly at the vertical CG location and the launch force will be acting directly parallel to the aircraft's orientation, as shown in Figure 23.

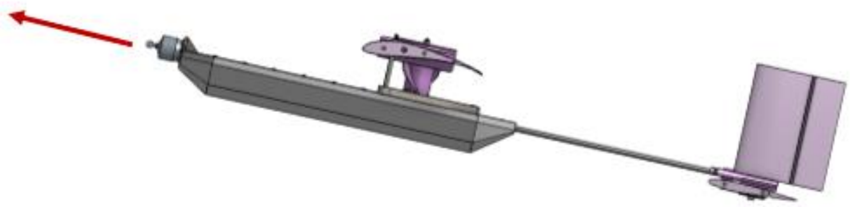

Figure 23: Launch Force Assumption

By using this assumption, a maximum tensile force and tensile stress were found in order to determine whether our fuselage was strong enough to endure the force of launch.

The results of both of these sets of analysis are shown in Table 11.

Table 11: Fuselage Analysis Results

Parameter	Value	Units
Maximum Landing Stress	5890	psi
Ultimate Landing Strength	9000	psi
Maximum Launch Stress	131	psi
Ultimate Launch Strength	3000	psi

As these results clearly show, our aircraft's fuselage is well-designed to adequately withstand our launch force, and reasonably able to withstand a controlled belly landing at a worst-case location on the fuselage. Worth noting is that the foam-board surrounding the bottom surface of our fuselage was not considered in this particular analysis, but would considerably help lowering the stress endured by the wooden channel by absorbing some of the impact by compression. While some damage may occur to the foam board itself from this kind of impact, the main structure of the fuselage would remain intact. In addition, we are prepared to administer small repairs to the foam board, if necessary, and may even bring a spare foam board skin in order to replace the entire fuselage surface if absolutely necessary.

Summary

In summary, each of these sets of analysis were intended to reduce structural members to as low a weight as possible while still ensuring that our aircraft will not break under any loading conditions considered within a reasonable range of our mission parameters. In addition, we were able to significantly reduce material costs by sizing our main wing spars and tail boom to be from the same size of carbon fiber tube.

Dynamics and Controls

This section of the report will focus on the dynamics and control aspect of an aircraft design. The analysis of the dynamics and control demonstrates that the aircraft will fly and meet level 1 flying qualities as it was reported in RFP. The horizontal and vertical tails of the aircraft will be important in stabilizing the aircraft and the control surfaces, which are elevator, ailerons, and rudder, are also important in the dynamic stability of aircraft.

Control Surface Sizing (Class 1 sizing)

The sizes of the control surfaces, elevator, rudder, and ailerons, were determined using Class 1 sizing method. The historical data that we used was obtained from Roskam Part 2 Chapter 8[1], where horizontal tail volume, vertical tail volume, and the data of aileron and elevator of homebuilt airplanes were provided. Using this historical data from Roskam, the area of the elevator, rudder and ailerons for our aircraft design were calculated.

Table 12: Elevator, Rudder, and Ailerons area ratio from historical data

Elevator		Rudder		Ailerons	
S_h/S_w	S_e/S_h	S_v/S_w	S_r/S_w	S_a/S_w min	S_a/S_w max
0.147	0.460	0.067	0.030	0.063	0.14

For the area of the elevator, we computed the ratio of the horizontal tail area to wing area of each homebuilt airplanes from the historical data. Then, S_h/S_w of our design was calculated, which was 0.153, and choose the ratio from the historical data that was close to our value, which is presented in Table 12. Then, we used its corresponding ratio of elevator to the horizontal tail area and calculated the size of the elevator for our aircraft design, $S_e = 51.55 in^2$.

For the area of the rudder, we computed the ratio of the vertical tail area to the wing area and the ratio of the rudder area to the wing area of each homebuilt airplanes from the historical data. Then, we computed S_v/S_w of our design, which was 0.062, and choose the ratio from historical data that was close to our value. Then, we took its corresponding rudder area to wing area ratio and calculated the size of the rudder for our aircraft design, $S_r = 21.89\ in^2$.

For the area of ailerons, we found the minimum and maximum values of the ratio of the ailerons area to wing area. Within this range, we choose S_a/S_w 0.10 from the historical data. Using this ratio 0f 0.10, we obtained the ailerons' size for our aircraft design, $S_a = 73.15\ in^2$.

Tail Sizing (Class 2 sizing)

We used Class 2 sizing of horizontal and vertical tail using X-plots. The Class 2 sizing method was consisted of longitudinal X-plot for the horizontal tail and directional X-plot for the vertical tail.

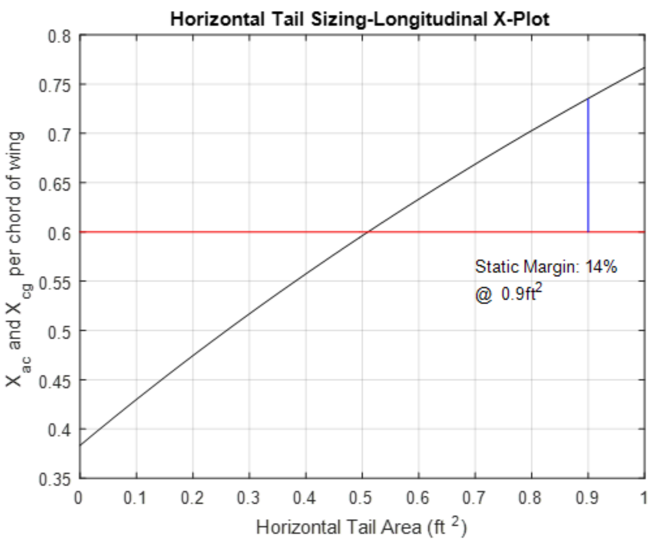

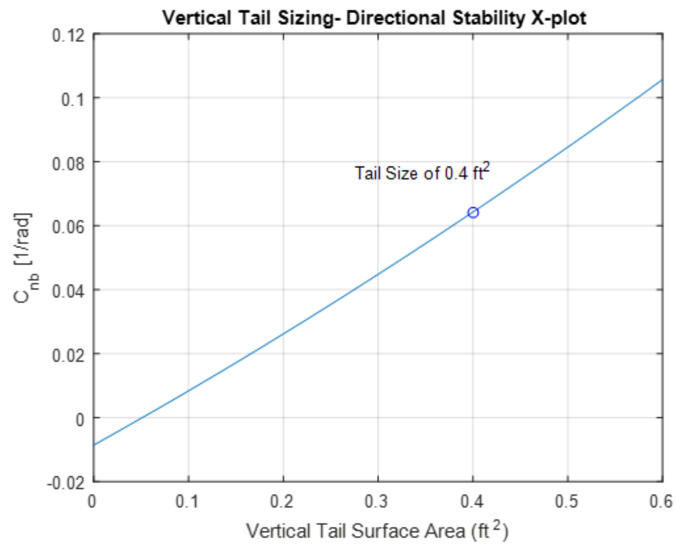

Figure 24: Longitudinal X-Plot

Figure 25: Directional Stability X-Plot

The longitudinal X-plot, which displayed the static longitudinal stability characteristic, was plotted with the center of gravity line that represented the rate at which the center of gravity moves to the aft and the aerodynamic center line that represented the rate at which the aerodynamic center moves to the aft. We had the center of gravity location at the 0.6 per chord from the leading edge. These two legs were plotted as a function of horizontal tail area. From this longitudinal X-Plot, the horizontal tail area of 0.9 ft^2(130 in^2), which was an approximated value of our aircraft's horizontal tail area, corresponded to the static margin of 14%. From Roskam, it suggested the static margin to be between 10% and 15%, which showed that our static margin was in the desirable range.

The directional stability X-plot, which displayed the static directional stability characteristic, was plotted as a function of vertical tail area. From this directional stability X-plot, the vertical tail area of 0.4 ft^2(57.6 in^2), which was an approximated value of our aircraft vertical tail area, presented the C_{nb} of 0.064/rad., which was equivalent to 0.001/deg. When the overall level of directional stability was approximately 0.0010 per degree, the Roskam Part II chapter 11[2] stated that the aircraft would be inherently directionally stable. Our C_{nb} value was close to 0.001/deg., which told us that our aircraft design would be inherently directionally stable.

Aerodynamic Center and Center of Gravity

The following Figure 26 presented position of the aerodynamic center for wing and body and the position of the aerodynamic center for horizontal tail. We got the aerodynamic center for wing and body at 4.56 inch from the leading edge and the aerodynamic center for the horizontal tail at 27.80 inch from the leading edge.

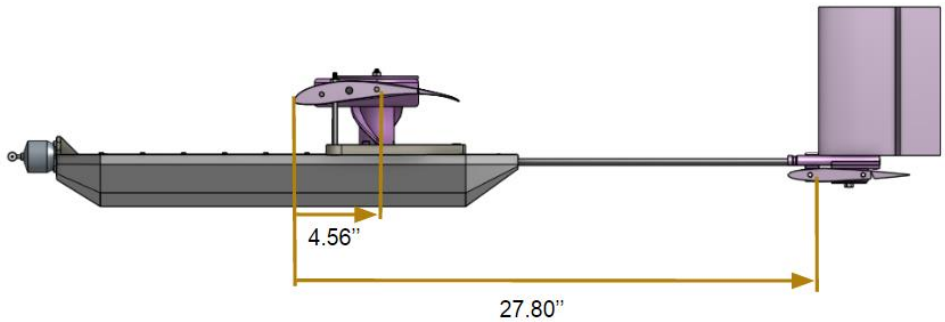

Figure 26: Location of Forward and Aft Center of Gravity

Summary

In summary, class 2 sizing is used to present that our aircraft will be stable during flight. Because our aircraft is inherently stable for pitch stability and yaw stability and neutrally stable for roll stability, a feedback controller will not be required.

Overall Design and Conclusion

With the system we have designed, our total expenditure for the design, testing, and building of our aircraft totaled $256.19. This expenditure fell slightly under our estimated expenditure of $269.05 and well under our RFP requirement of $300. A detailed budget can be found in the appendix.

The wing deployment mechanism in our design is unique and robust. The entire component is fabricated using additive manufacturing and this design has not been implemented in any other UAV design to date. The complexity of the wing-deployment mechanism increases the weight of the UAV which is a weakness in the design; however, the propulsion system is adequately sized to fly the UAV at this heavier weight. The complexity of the component also reduces the reliability and assurance that the component will act as designed.

A folding propeller is also used in the design which is beneficial to avoid any damage done to the propeller when performing the required belly landing. The folding propeller requires a larger motor which increases the weight of the UAV, but this is a small disadvantage because the increased weight due to the motor and battery provide enough power and energy to adequately fly the UAV and power the internal components.

The structural components of the aircraft have been sized and designed to not break under maximum loading conditions during flight or during a belly-landing as required from the RFP. In addition to not breaking, they have also been designed from materials in order to reduce the overall weight of the aircraft as much as possible in order to meet the RFP requirement of being as light as practical. Overall, the UAV has been engineered to complete the flight mission as required by the RFP.

References

1. J. Roskam. (1985). Airplane Design: Parts II: Preliminary Configuration Design And Integration of the Propulsion System, Lawrence, Kansas : Roskam Aviation and Engineering Corporation.
2. J. Roskam. (1987). Airplane Design: Part VI: Preliminary Calculation of Aerodynamic, Thrust And Power Characteristics, Lawrence, Kansas: Roskam Aviation and engineering Corporation.

Appendix

Concept Selection

The following are our morphological matrices that define our three initial design concepts by their various unique characteristics. These were brainstormed as a team and were our primary starting points for proposing potential designs.

Concept 1 (Green Highlighted Items)				
	Characteristics	**Alternative 1**	**Alternative 2**	**Alternative 3**
Propulsion	Number of blades	2	3	4
	Propulsion Type	fixed propeller	EDF	folding propeller
	Gearbox	Yes	No	
	Number of Propulsive Systems	1	2	3
Aerodynamics	Wing Type	Conventional Wing (Folding)	Fabric / Conventional Wing (Folding)	
	High lift devices	Conventional Flaps	Flaperons	None
	Number of main wings	1	2	2 - Connected
	Wing Planform	Rectangular	Tapered	Elliptical
	Swept angle	Yes	No	
Structures	General Structure	Ribs & Spars	Ribs & Strong skin	Ribs, Spars & Strong skin
	Material	UltraCote and Wood	Composites and Foam	Composites and Nylon Taffeta
	Joints	Welding	Glue	Nut & Bolt
	Fuselage	Cylindrical	Rectangular	Triangular
Control	Controlling Surfaces	Conventional tail	T-tail	V-tail
	Roll stability	Dihedral Angled	Control System	

Concept 2 (Blue Highlighted Items)				
	Characteristics	**Alternative 1**	**Alternative 2**	**Alternative 3**
Propulsion	Number of blades	2	3	4
	Propulsion Type	fixed propeller	EDF	folding propeller
	Gearbox	Yes	No	
	Number of Propulsive Systems	1	2	3
Aerodynamics	Wing Type	Conventional Wing (Folding)	Fabric / Conventional Wing (Folding)	
	High lift devices	Conventional Flaps	Flaperons	None
	Number of main wings	1	2	2 - Connected
	Wing Planform	Rectangular	Tapered	Elliptical
	Swept angle	Yes	No	
Structures	General Structure	Ribs & Spars	Ribs & Strong skin	Ribs, Spars & Strong skin
	Material	UltraCote and Wood	Composites and Foam	Composites and Nylon Taffeta
	Joints	Welding	Glue	Nut & Bolt
	Fuselage	Cylindrical	Rectangular	Triangular
Control	Controlling Surfaces	Conventional tail	T-tail	V-tail
	Roll stability	Dihedral Angled	Control System	

Concept 3 (Red Highlighted Options				
	Characteristics	**Alternative 1**	**Alternative 2**	**Alternative 3**
Propulsion	Number of blades	2	3	4
	Propulsion Type	fixed propeller	EDF	folding propeller
	Gearbox	Yes	No	
	Number of Propulsive Systems	1	2	3
Aerodynamics	Wing Type	Conventional Wing (Folding)	Fabric / Conventional Wing (Folding)	
	High lift devices	Conventional Flaps	Flaperons	None
	Number of main wings	1	2	2 - Connected
	Wing Planform	Rectangular	Tapered	Elliptical
	Swept angle	Yes	No	
Structures	General Structure	Ribs & Spars	Ribs & Strong skin	Ribs, Spars & Strong skin
	Material	UltraCote and Wood	Composites and Foam	Composites and Nylon Taffeta
	Joints	Welding	Glue	Nut & Bolt
	Fuselage	Cylindrical	Rectangular	Triangular
Control	Controlling Surfaces	Conventional tail	T-tail	V-tail
	Roll stability	Dihedral Angled	Control System	

Propulsion

Equations of Motion for Non-Accelerated Climb:

$$T - D - Wsin(\gamma) = 0 \quad \& \quad L - Wcos(\gamma) = 0$$

Equations of Motion for Cruise:

$$T - D = 0 \quad \& \quad L - W = 0$$

Thrust and Power Equations:

$$T_R = D = \frac{1}{2}\rho V^2 S C_D \quad T_A = \rho n^2 D^4 C_T$$

$$P_R = T_R V \quad P_A = T_A V$$

Power Required by Propeller:

$$P_{propeller} = \rho n^3 D^5 C_p$$

Power output by Motor:

$$P = (I_{in} - I_o) * (V_{in} - I_{in} * R_m)$$

Climb Angle:

$$\sin(\gamma) = \frac{T - D}{W}$$

Nomenclature:

T – Thrust   D – Drag   W – Weight   L – Lift   γ – Flight Path Angle
S – Surface Area C_D – Coefficient of Drag   ρ – Density   V – Velocity
C_T – Coefficient of Thrust C_P – Coefficient of Power I_o – Idle Current
Rm – Terminal Resistance

Energy Consumption:

E = Volt * Current * time (J)	14.8V * 3A-hr *(3600s/1hr) = 159,840 J
Climb	14.8V * 25A * 42.2s = 15,614 J
Cruise	14.8 V * 7.7 A * 8 min*(60s/min) = 54,700 J
Total Consumed	89,526 J
Percentage Used	56 %

Aerodynamics

XFLR5 Analysis

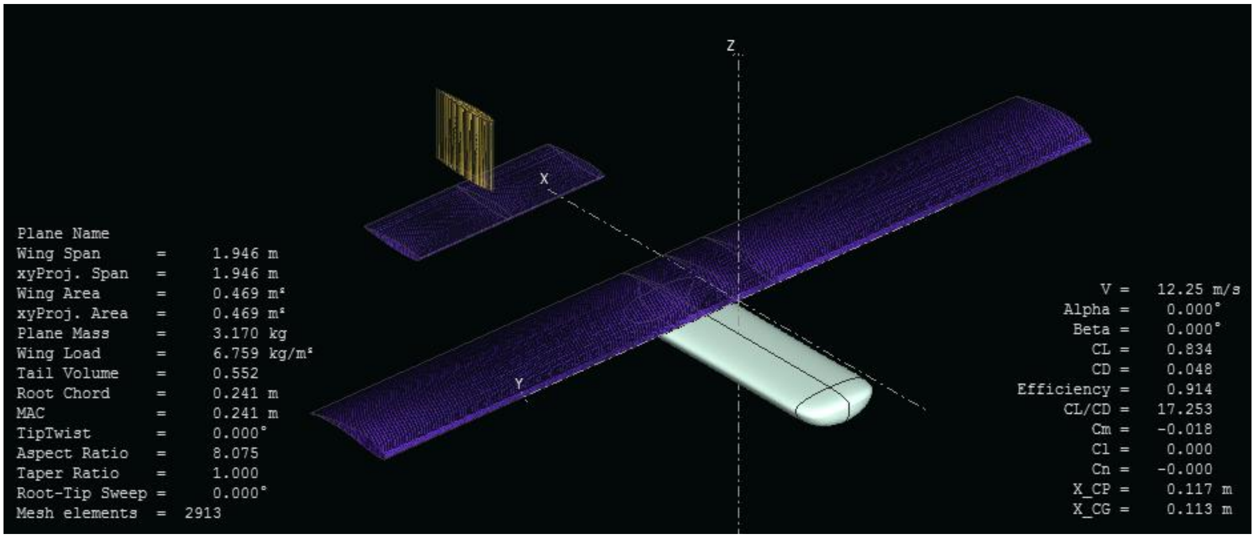

A preliminary XFLR5 analysis was performed in order to obtain a first approach to the aerodynamics data.

In this analysis a simplified CAD model was used which basically included main wings tail with both, horizontal and vertical stabilizers, and the fuselage, neglecting the wing deployment system and tail boom as they have a marginal contribution compared to the rest of the UAV.

Regarding to the flow conditions the simulation was carried under a free stream velocity of 38.9 ft/s (11.8 m/s).

The numerical solver model was Ring Vortex (Viscous).

CFD Data

Due to the limitations of XFLR5 software, CFD analysis is used to obtain reliable aerodynamic data.

A domain of 35 million cells was used with the following setup:

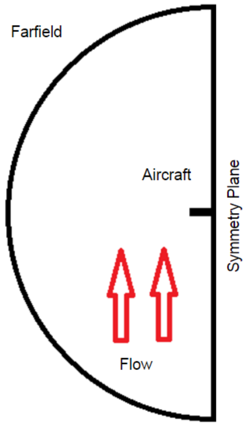

The flow conditions used were the same as the XFLR5 analysis (a free stream velocity of 38.9 ft/s).

The numerical solver is RANS with K-ε.

α (∘)	C_L	C_D	C_M
-5	0.01812	0.07713	-1.25
-4.5	0.07596	0.07082	-1.2009
-4	0.1265	0.06859	-1.1509
-3.5	0.1729	0.06583	-1.1093
-3	0.2188	0.06508	-1.059
-2.5	0.2645	0.065	-1.0183
-2	0.3052	0.06433	-1.0013
-1	0.3893	0.06663	-0.9539
0	0.4695	0.06968	-0.9068
1	0.5492	0.07251	-0.8926
2	0.6266	0.0781	-0.874
3	0.7061	0.08419	-0.8497
4	0.7802	0.09056	-0.8414
5	0.8511	0.1012	-0.864
6	0.9228	0.1105	-0.8902
7	0.9822	0.1236	-0.9503
8	1.046	0.1358	-0.9911
9	1.1001	0.151	-1.073
10	1.1583	0.1651	-1.1397
11	1.2141	0.1794	-1.1615
12	1.2584	0.1972	-1.3123
13	1.3184	0.2099	-1.3781
14	1.3733	0.2241	-1.3812
15	1.412	0.2386	-1.4967

Stability considerations for tail sizing

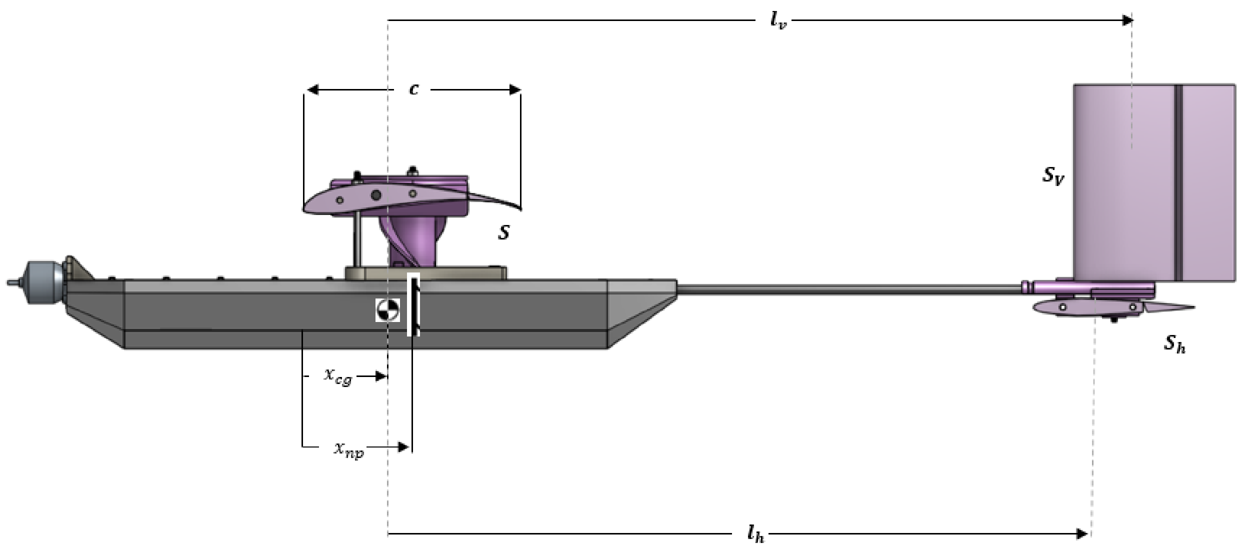

The neutral point is the location of the center of gravity of the aircraft at which at which the aircraft is longitudinally stable.

Analytically a preliminary neutral point can be calculated as:

$$x_{NP} = \frac{1}{4} + \frac{1 + \frac{2}{AR}}{1 + \frac{2}{AR_h}} \cdot \left(1 - \frac{4}{2 + AR}\right) \cdot V_h \cdot c$$

$$x_{NP} = 4.91\ in\ (from\ LE)$$

Note that the previous calculation of the neutral point has been performed only taking into account the main wing and the tail, but not the fuselage, so this location may slightly changes, after this contribution.

The numbers to do perform this calculation will be obtained in the next steps.

$$x_{CG} \equiv Centre\ of\ gravity\ location$$

A non-dimensional distance between the centre of gravity and the neutral point called Stability Margin (SM):

$$SM = \frac{x_{CG} - x_{NP}}{c}$$

A positive SM means the aircraft is stable but as we get close to zero the manoeuvrability keeps increasing up to when SM is a negative scalar, then the aircraft is unstable. It can be visualized in the following figure:

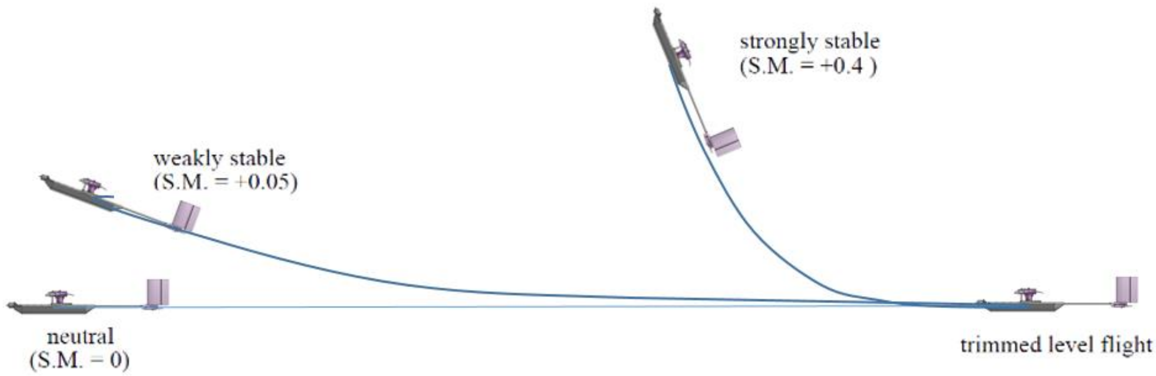

According to Historical Data a desirable range of SM values would be:

$$SM \in [0.05, 0.15]$$

Which would give us a range of centre of gravity locations of:

$$x_{CG} \in [0.38, 0.47]\ in\ (from\ LE)$$

Volume coefficients for horizontal and vertical tail

Knowing these parameters. the tail can be sized according to the volume coefficients for horizontal and vertical tails:

$$V_h = \frac{S_h l_h}{Sc}$$

$$V_v = \frac{S_v l_v}{Sb}$$

Where:

$$S_h \equiv Horizontal\ tail\ total\ surface$$

$$S_v \equiv Vertical\ tail\ total\ surface$$

$$l_h \equiv Arm\ to\ the\ horizontal\ tail$$

$$l_v \equiv Arm\ to\ the\ vertical\ tail$$

$$S \equiv Wing\ surface\ area$$

$$c \equiv Wing\ chord$$

$$b \equiv Wing\ span$$

(See previous page sketch)

Horizontal stabilizer volume coefficient

As $V_h \to 0$ the aircraft is more sensitive to changes in CG location, so that the pitch controllability will be more complicated.

According to historical data an aircraft with good stability characteristics will have:

$$V_h \in [0.4, 0.7]$$

In order to be conservative this aircraft is designed to achieve:

$$V_h = 0.6$$

Vertical stabilizer volume coefficient

In an analogous way, as the aircraft is more sensitive to yawing (Dutch roll), so again a trade-off must be reached. According to historical data $V_v \in [0.03, 0.06]$. This aircraft is designed to achieve $V_v = 0.05$

Structures

Maximum Loading Conditions

In order to determine our maximum loading conditions, we began by calculating our maximum load factor during a sharply banked turn using the following equations:

$$\varphi = tan^{-1}\left(\frac{V^2}{rg}\right) = tan^{-1}\left(\frac{46^2}{35*32.2}\right) = 62.0° \qquad n = \frac{SF}{\cos(\varphi)} = \frac{1.5}{\cos(62.0°)} = 3.19$$

□	bank angle of turn	r	radius of turn	SF	safety factor
V	velocity of turn	g	gravitational acceleration	n	maximum load factor

This also correlated with our V-n diagram, which indicated our maximum load factor under gusting wind conditions to be 3.19 as well.

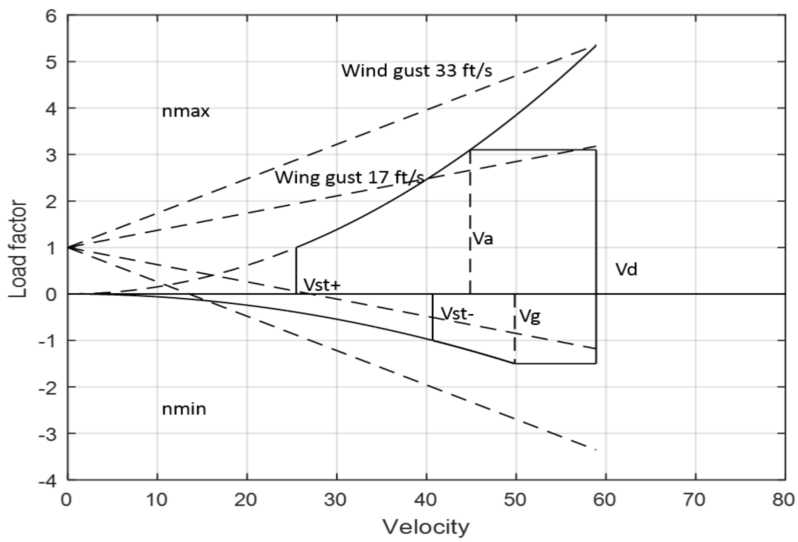

We then determined the maximum lifting force our aircraft would produce from both wings from our maximum load factor using our aircraft's estimated weight and the following equation:

$$L = nW = 1.5 * 7.4 = 23.6\ lbf$$

L	maximum lift force	n	maximum load factor	W	weight of aircraft

Finally, we were able to calculate the maximum bending moment acting on each wing by using the following equation:

$$M = \frac{L}{2} * \frac{b}{4} = \frac{23.6}{2} * \frac{68}{4} = 200.7\ lbf - in$$

M	maximum bending moment	L	maximum lift force	b	span of wings

Spar Analysis

We began by determining the second moment of inertia of our intended carbon fiber tubes using the following equation:

$$I = \frac{\pi(r_2^4 - r_1^4)}{4} = \frac{\pi(0.187^4 - 0.148^4)}{4} = 0.000587\ in^4$$

I	second moment of inertia	r_2	outer radius of tube	r_1	inner radius of tube

We then determined the maximum stress undergone by the spar by using the following equation:

$$\sigma = \frac{My}{I} = \frac{200.7 * 0.187}{0.000587} = 67258\ psi$$

□	bending stress	M	maximum bending moment
y	vertical height above axis	I	second moment of inertia

Finally, we calculated the maximum deflection and deflection angle from the following two equations:

$$\delta = \frac{Ll^3}{8EI} = \frac{23.6 * 34^3}{8 * 22000000 * 0.000587} = 4.49\ inches \qquad \theta_d = \frac{\delta}{l} = \frac{4.49}{34} = 7.56°$$

□	maximum deflection	L	maximum lift force	l	length of wing
E	Young's modulus	I	second moment of inertia	$□_d$	deflection angle

Skin Thickness Analysis

We began by determining the minimum second moment of inertia needed to endure our maximum bending moment and then found the minimum skin thickness required to meet this minimum moment of inertia using the following equations and a MATLAB loop*:

$$I = \frac{My}{\sigma_{max}} = \frac{200.7 * 1}{60000} = 0.0033\ in^4 \qquad I = \frac{ch^3}{12} - \frac{(7 - 2 * t)(2 - 2 * t)^3}{12}$$

$□_{max}$	fiberglass strength	c	rectangular width
h	rectangular height	t	skin thickness

Next, we determined the necessary section modulus needed to endure a maximum torsional force and then determined the minimum skin thickness required to meet this section modulus using the following equations and several MATLAB loops*:

$$\varphi = \frac{T\ell}{GJ_T} \quad G = \frac{E}{2(1+\nu)} \quad J = \frac{2c^2h^2t}{c+h} \quad T_{max} = \frac{1}{2}\rho S V_{max}^2 C_m c$$

□	maximum twist angle	T	torsional force	l	half of rectangular base
G	shear modulus	J	section modulus	□	Poisson's ratio
□	air density	S	cross-sectional area	C_m	moment coefficient

Tail Boom Analysis

We used the same process as our Spar Analysis in order to determine the maximum stress and deflections of our tail boom during in-flight loading, but with a different moment equation and different values:

$$M = Fx = 10 * 18 = 180\ lbf - in \qquad \sigma = \frac{My}{I} = \frac{180 * 0.187}{0.000587} = 60319\ psi$$

$$\delta = \frac{Fx^2 * a}{6EI} = \frac{10 * 20^3 * 18}{6 * 22000000 * 0.000587} = 1.51\ in \qquad \theta_d = \frac{\delta}{l} = \frac{1.51}{34} = 4.21°$$

F	maximum deflection force	x	force application point	a	distance modifier

In addition, we used the same process again to analyze our landing impact, but used the following equations to determine our landing force:

$$V_y = V_{cruise} sin(\theta) = 38.9 * sin(3°) = 2.04\ ft/sec$$

$$F_{landing} = \frac{SF \frac{1}{2} m V_y^2}{dy} = \frac{1.5 * \frac{1}{2} * 0.2298 * 2.04^2}{1} = 8.57\ lbf$$

$$F_{friction} = F_{landing} \mu = 8.57 * 0.1 = 0.857\ lbf$$

$$F_{net} = F_{friction} \sin(\theta)\, F_{landing} \cos(\theta) = 0.857 \sin(3°)\, 8.57 \cos(3°) = 8.61\ lbf$$

V_y	vertical velocity	□	landing angle	m	aircraft mass
dy	absorption distance	□	friction coefficient		

Fuselage Analysis

We used the same landing force generated by our Tail Boom Landing Analysis, but placed it in the center of our bottom channel in order to determine the maximum moment and stress encountered by the channel during landing using the following equations:

$$M = Fx = 10 * 12.6/2 = 54\ lbf - in \qquad I = \frac{bh^3}{12} = \frac{0.22 * 0.5^3}{12} = 0.0023 in^4$$

$$\sigma = \frac{M \frac{h}{2}}{I} = \frac{54 * \frac{0.5}{2}}{0.0023} = 5892\ psi$$

b	support width	h	support height

***** MATLAB code available upon request to Alex Sechtig (asechtig@purdue.edu)

Dynamics and Controls:

Control Surface Sizing (Class 1 sizing)

Historical data from Roskam and computed ratio used for class 1 sizing of control surfaces:

Historical data of control surfaces: Elevator

Wing Area (S_w)[ft^2]	Horizontal Tail Area (S_h)[ft^2]	S_h/S_w	S_e/S_h
76.400	10.400	0.136	0.450
77.500	14.500	0.187	0.600
80.700	13.400	0.166	0.520
80.700	15.400	0.191	0.480
81.000	11.700	0.144	0.250
96.700	19.400	0.201	0.140
104.000	22.500	0.216	0.500
112.000	**16.500**	**0.147**	**0.460**
118.000	23.500	0.199	0.510
119.000	22.200	0.187	0.330
125.000	25.400	0.203	0.490
130.000	25.500	0.196	0.430
135.000	26.000	0.193	0.520

Historical Data of Control Surfaces: Rudder

Wing Area (S_w)[ft^2]	Vertical Tail Area (S_v) [ft^2]	S_v/S_w	S_r/S_v	S_r/S_w
76.4	3.49	0.046	0.330	0.015
77.5	4.36	0.056	0.670	0.038
80.7	11.3	0.140	0.420	0.059
80.7	6.86	0.085	0.380	0.032
81	7.15	0.088	0.310	0.027
96.7	6.89	0.071	0.240	0.017
104	7.64	0.073	0.500	0.037
112	**7.53**	**0.067**	**0.440**	**0.030**
118	9.49	0.080	0.550	0.044
119	8.35	0.070	0.300	0.021
125	6.73	0.054	0.710	0.038
130	16.5	0.127	0.310	0.039
135	11.7	0.087	0.350	0.030

Historical Data of Control Surfaces: Aileron

Wing Area (S_w)[ft^2]	Wing Span (b)[ft^2]	S_a/S_w
76.4	17	0.13
119	28.7	0.063

118	26.4	0.077
104	23.6	0.092
80.7	20.3	0.067
77.5	19.4	0.082
80.7	21.3	0.08
81	27	0.14
112	25	0.13
130	30	0.085
125	25	0.11
135	30	0.097
96.7	19.3	0.083

Tail Sizing (Class 2 sizing)

The following equations, from Roskam, are used for the longitudinal X-plot:

$$\bar{x}_{ac_A} = \frac{1}{F}\left[\bar{x}_{ac_{wb}} + \left\{C_{L_{\alpha_h}}\left(1 - \frac{d\varepsilon_h}{d\alpha}\right)\left(\frac{S_h}{S}\right)\bar{x}_{ac_h}\right\}\right]$$

$$F = \left[1 + \frac{1}{C_{L_{\alpha_{wb}}}}\left\{C_{L_{\alpha_h}}\left(1 - \frac{d\varepsilon_h}{d\alpha}\right)\left(\frac{S_h}{S}\right)\right\}\right.$$

$\bar{x}_{ac_A}$	The aerodynamic center leg that represents the rate at which the aerodynamic center moves aft/forward as a function of horizontal tail area
$\bar{x}_{ac_{wb}}$	Aerodynamic center for wing-body
$C_{L_{\alpha_h}}$	Lift coefficient alpha for win-body
S_h	Horizontal tail area

The following equations, from Roskam, are used for the directional X-plot:

$$C_{n_\beta} = C_{n_{\beta_w}} + C_{n_{\beta_f}} + C_{n_{\beta_v}}$$

$$C_{n_{\beta_w}} = 0$$

$$C_{n_{\beta_f}} = -57.3\, K_N K_{R_l}\left(\frac{S_{f_s} l_f}{S * b}\right)$$

$$C_{n_{\beta_v}} = -(C_{y_{\beta_v}})\,\frac{(l_v\cos\alpha + z_v\sin\alpha)}{b}$$

$$C_{y_{\beta_v}} = -K_v(C_{L_{\alpha_v}})\left(1 + \frac{d\alpha}{d\beta}\right)\eta_V\left(\frac{S_V}{S}\right)$$

$$\left(1 + \frac{d\alpha}{d\beta}\right)\eta_V = 0.724 + 3.06\left(\frac{S_v/S}{2}\right) + 0.4\left(\frac{z_w}{z_f}\right) + 0.009A$$

$$C_{L_{\alpha_w}} = \frac{2\pi A}{\left[2 + \left(\frac{A^2\beta^2}{k^2} + 4\right)^{\frac{1}{2}}\right]}$$

Following table shows the constants that is used for the directional X-plot. Some of the constants like empirical factor were obtained using the plots from Roskam textbook.

K_v (empirical factor)	0.85	
K_N	0.0002	
K_{R_l}	1.02	
l_v (for locating vertical tail)	2.25	ft
z_v (for locating vertical tail)	0.1875	ft
S_{f_s} (side body area)	0.5625	ft^2
l_f (fuselage length)	4.25	ft
z_w (wing distance to fuselage centerline)	0.25	ft
z_f (vertical height of fuselage at wing root chord)	0.25	ft

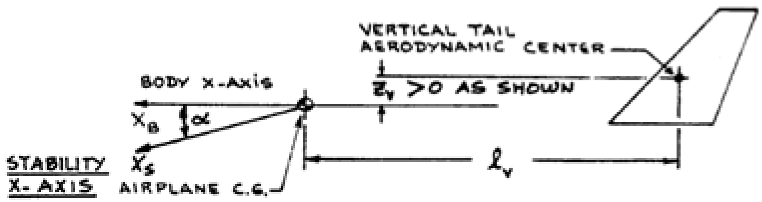

Geometry for Locating Vertical Tail(s)

Budget

Subsystem	Item	Budget	Actual	Subsystem	Item	Budget	Actual
Main Wing	Foam	$30.00	$38.11	Electronics	Camera	$25.00	$17.79
	Fiberglass	$0.00	$0.00		GPS/Altimeter	$0.00	$0.00
	Carbon Fiber Spars	$28.00	$28.45		Receivers	$0.00	$0.00
	Wood Spars	$0.00	$3.18				
Wing Deployment	3D Printed Mechanism	$16.79	$16.79		Servos	$20.00	$0.00
	Slider Bar	$30.36	$35.72		Wiring	$6.00	$0.00
	Magnets	$0.00	$5.39				
Fuselage	Foam-board	$14.98	$11.02	Launch system	Launch Tube	$20.00	$18.44
	Plywood Ribs/Baseplates	$12.00	$12.42		Fishing Line	$6.99	$5.47
Tail	Foam	$0.00	$0.00		Surgical Tubing	$20.44	$15.76
	Fiberglass	$0.00	$0.00		Stake	$2.49	$2.98
	Tail Boom	$0.00	$0.00	Miscellaneous	Adhesives	$0.00	$5.39
	3D Printed Mechanism	$0.00	$0.00		Nuts/Bolts	$7.00	$6.36
Propulsion System	Propeller	$0.00	$0.00				
	Motor	$0.00	$0.00		**TOTAL**	$269.05	$256.19
	Speed Controller	$0.00	$0.00				
	Battery Pack	$29.00	$32.92				